articles

molecular pharmaceutics

# Molecular Basis of Inactive B-RAF$^{WT}$ and B-RAF$^{V600E}$ Ligand Inhibition, Selectivity and Conformational Stability: An *in Silico* Study

**Filip Fratev,*,† Svava Ósk Jónsdóttir,† Elina Mihaylova,‡ and Ilza Pajeva§**

*Center for Biological Sequence Analysis, Department of Systems Biology, Technical University of Denmark, Kemitorvet, Building 208, DK-2800 Kongens Lyngby, Denmark, Micar Ltd., 39 Asparuh Str., 1000 Sofia, Bulgaria, and Centre of Biochemical Engineering "Ivan Daskalov", Bl. 105 Acad G. Bontchev Str., 1113 Sofia, Bulgaria*

Received July 28, 2008; Revised Manuscript Received November 7, 2008; Accepted November 11, 2008

**Abstract:** The B-RAF kinase plays an important role both in tumor induction and maintenance in several cancers. The molecular basis of the inactive B-RAF$^{WT}$ and B-RAF$^{V600E}$ inhibition and selectivity of a series of inhibitors was examined with a combination of molecular dynamics (MD), free energy MM-PBSA and local-binding energy (LBE) approaches. The conformational stability of the unbounded kinases and in particular the processes of the B-RAF$^{V600E}$ mutant activation were analyzed. A unique salt bridge network formed mainly by the catalytic residues was identified in the unbounded B-RAFs. The reorganization of this network and the restriction of the active segment flexibility upon ligand binding inhibit both B-RAF$^{WT}$ and B-RAF$^{V600E}$, thus appearing as an important factor for ligand selectivity. A significant correlation between the binding energies of the compounds in B-RAF$^{WT}$ and their inhibition effects on B-RAF$^{V600E}$ was revealed, which can explain the low mutant selectivity observed for numerous inhibitors. Our results suggest that the interactions between the activation segment and the αC-helix, as well as between the residues in the salt bridge network, are the major mechanism of the B-RAF$^{V600E}$ activation. Overall data revealed the important role of Lys601 for ligand activity, selectivity and protein stabilization, proposing an explanation of the observed strong kinase activation in the K601E mutated form.

**Keywords:** B-RAF; molecular dynamics; MM-PBSA; docking; LBE; kinases

## 1. Introduction

The success of novel cancer therapies depends on the identification of functional targets that play an essential role in tumor growth and survival. Constitutive activation of the RAF-MEK-ERK pathway is common to numerous cancers.[1] As a member of the RAF kinase group, B-RAF is important both in tumor induction and in maintenance. Therefore, it is an important and exciting new therapeutic target for several human cancers. Recently, large-scale genomic screens have detected mutations in B-RAF in 66% of malignant melanomas and at a lower frequency in colorectal and ovarian cancers.[2] Other cancer types have been found to harbor B-RAF mutations, and over 40 mutations have been identified.[3,4] Most of the mutations of B-RAF are clustered in two different regions within the binding pocket: one is the glycine-rich P loop (P-loop) of the N lobe, and the other one is the activation segment (A-loop). A Val to Glu substitution at residue 600 in the activation segment, adjacent to the conserved DFG motif, accounts for 90% of B-RAF mutations in human cancers. B-RAF$^{V600E}$ has a 500-fold

* Corresponding author. Mailing address: Technical University of Denmark, Center for Biological Sequence Analysis, Kemitorvet, Building 208, DK-2800 Kongens Lyngby, Denmark. Phone: +45 45252477. Fax: +39 45931585. E-mail: fratev@cbs.dtu.dk.

† Technical University of Denmark.

‡ Micar Ltd.

§ Centre of Biochemical Engineering "Ivan Daskalov".

(1) Malumbres, M.; Barbacid, M. RAS oncogenes: the first 30 years. *Nat. Rev. Cancer* **2003**, *3*, 459–465.



**10.1021/mp8001107 CCC: $40.75** 
Published on Web 12/02/2008

higher kinase activity, relative to the basal activity of the wild type protein (B-RAF$^{WT}$), providing cancer cells with both proliferation and survival signals and allowing them to grow as tumors in model systems.[4] Several other mutations provoke high kinase activity and were classified as "strongly activating". These are V600D, V600K, V600R, G469A and K601E.[4]

Crystal structures of the B-RAF$^{WT}$ and B-RAF$^{V600E}$ kinase binding domains have been solved, adding to the understanding of mechanism involved in B-RAF activation.[4] Recently, the structures of the active form of B-RAF (B-RAF-A) were obtained.[5,6] It has been suggested that the molecular interactions between the P and A-loops in B-RAF$^{WT}$ stabilize the inactive form, and that the substrate recognition leads to conformational changes that set the catalytic cleft free and allows the enzyme to achieve a full active state.[4,7] In particular, interactions between Phe468 in the P-loop and Val600 in the A-loop were identified. It has been predicted that the mutation of Val600 to a larger and more charged residue will lead to the A-loop destabilization, flipping it to the active position.[4] However, in the newly obtained crystal structures of the inactive B-RAF$^{WT}$,[6] the position and orientation of Phe468 significantly differ from those previously solved. Several other mutations need further elucidation, as, for example, the strong B-RAF activation by the K601E mutation. Although most B-RAF mutants display elevated kinase activity compared to the wild type protein, four cancer-derived mutants have reduced kinase activity.[3] Three of these mutations (B-RAF$^{G466E}$, B-RAF$^{G466V}$ and B-RAF$^{G596R}$) are capable of inducing ERK phosphorylation through heterodimerization with C-RAF. The fourth mutant (B-RAF$^{D594V}$) acts like a kinase-dead mutant and cannot bind to C-RAF. Its role in tumorigenesis remains to be elucidated.[3] These findings point to the important role of particular amino acids and suggest further elucidation of the molecular basis for activation of the various B-RAF mutants. Additionally, MD simulations of B-RAF$^{WT}$, B-RAF$^{V600E}$ and B-RAF$^{V599Ins}$ showed that the electrostatic interactions between the P and A-loops and the αC-helix are an important factor for stabilization as well destabilization of the B-RAF conformation. The particular contribution of the αC-helix to these processes has not been specified yet.[8]

A number of B-RAF inhibitors that bind to either the inactive or the active B-RAF forms have been proposed, but apparently the B-RAF$^{V600E}$ selective inhibitors bind to the mutant in its active state.[5,6] It was shown, for example, that BAY43-9006 (Sorafenib) can only bind to the inactive B-RAF$^{WT}$ and B-RAF$^{V600E}$ and has identical binding mode and similar activity in both proteins,[4,9] whereas other inhibitors like SB-590885 and PLX4720 are highly selective to B-RAF$^{V600E}$ and bind to its active form.[5,6] However, comparable potency between the mutant, wild type and many other kinases has been reported for numerous inhibitors.[10−12] Obviously, elucidation of the mechanism of inhibition in the

(2) Davies, H.; Bignell, G. R.; Cox, C.; Stephens, P.; Edkins, S.; Clegg, S.; Teague, J.; Woffendin, H.; Garnett, M. J.; Bottomley, W.; Davis, N.; Dicks, E.; Floyd, Y.; Gray, K.; Hall, S.; Hawes, R.; Hughes, J.; Kosmidou, V.; Menzies, A.; Mould, C.; Parker, A.; Stevens, C.; Watt, S.; Hooper, S.; Wilson, R.; Jayatilake, H.; Gusterson, B. A.; Cooper, C.; Shipley, J.; Hargrave, D.; Pritchard-Jones, K.; Maitland, N.; Chenevix-Trench, G.; Riggins, G. J.; Bigner, D. D.; Palmieri, G.; Cossu, A.; Flanagan, A.; Nicholson, A.; Ho, J. W.; Leung, S. Y.; Yuen, S. T.; Weber, B. L.; Seigler, H. F.; Darrow, T. L.; Paterson, H.; Marais, R.; Marshall, C. J.; Wooster, R.; Stratton, M. R.; Futreal, P. A. Mutations of the BRAF gene in human cancer. *Nature* **2002**, *417*, 949–954.

(3) Michaloglou, C.; Vredeveld, L. C. W.; Mooi, W. J.; Peeper, D. S. BRAFE600 in benign and malignant human tumours. *Oncogene* **2008**, *27*, 877–895.

(4) Wan, P. T.; Garnett, M. J.; Roe, S. M.; Lee, S.; Niculescu-Duvaz, D.; Good, V. M.; Jones, C. M.; Marshall, C. J.; Springer, C. J.; Barford, D.; Marais, R. Mechanism of activation of the RAF-ERK signaling pathway by oncogenic mutations of B-RAF. *Cell* **2004**, *116*, 855–867.

(5) King, A. J.; Patrick, D. R.; Batorsky, R. S.; Ho, M. L.; Do, H. T.; Zhang, S. Y.; Kumar, R.; Rusnak, D. W.; Takle, A. K.; Wilson, D. M.; Hugger, E.; Wang, L.; Karreth, F.; Lougheed, J. C.; Lee, J.; Chau, D.; Stout, T. J.; May, E. W.; Rominger, C. M.; Schaber, M. D.; Luo, L.; Lakdawala, A. S.; Adams, J. L.; Contractor, R. G.; Smalley, K. S.; Herlyn, M.; Morrissey, M. M.; Tuveson, D. A.; Huang, P. S. Demonstration of a genetic therapeutic index for tumors expressing oncogenic BRAF by the kinase inhibitor SB-590885. *Cancer Res.* **2006**, *66*, 11100–11105.

(6) Tsai, J.; Lee, J. T.; Wang, W.; Zhang, J.; Cho, H.; Mamo, S.; Bremer, R.; Gillette, S.; Kong, J.; Haass, N. K.; Sproesser, K.; Li, L.; Smalley, K. S.; Fong, D.; Zhu, Y. L.; Marimuthu, A.; Nguyen, H.; Lam, B.; Liu, J.; Cheung, I.; Rice, J.; Suzuki, Y.; Luu, C.; Settachatgul, C.; Shellooe, R.; Cantwell, J.; Kim, S. H.; Schlessinger, J.; Zhang, K. Y.; West, B. L.; Powell, B.; Habets, G.; Zhang, C.; Ibrahim, P. N.; Hirth, P.; Artis, D. R.; Herlyn, M.; Bollag, G. Discovery of a selective inhibitor of oncogenic B-Raf kinase with potent antimelanoma activity. *Proc. Natl. Acad. Sci. U.S.A.* **2008**, *105*, 3041–3046.

(7) Dibb, N. J.; Dilworth, S. M.; Mol, C. D. Switching on kinases: oncogenic activation of BRAF and the PDGFR family. *Nat. Rev. Cancer* **2004**, *4*, 718–727.

(8) Moretti, S.; Macchiarulo, A.; De Falco, V.; Avenia, N.; Barbi, F.; Carta, C.; Cavaliere, A.; Melillo, R. M.; Passeri, L.; Santeusanio, F.; Tartaglia, M.; Santoro, M.; Puxeddu, E. Biochemical and molecular characterization of the novel BRAF(V599Ins) mutation detected in a classic papillary thyroid carcinoma. *Oncogene* **2006**, *25*, 4235–4240.

(9) Wilhelm, S. M.; Carter, C.; Tang, L.; Wilkie, D.; McNabola, A.; Rong, H.; Chen, C.; Zhang, X.; Vincent, P.; McHugh, M.; Cao, Y.; Shujath, J.; Gawlak, S.; Eveleigh, D.; Rowley, B.; Liu, L.; Adnane, L.; Lynch, M.; Auclair, D.; Taylor, I.; Gedrich, R.; Voznesensky, A.; Riedl, B.; Post, L. E.; Bollag, G.; Trail, P. A. BAY 43−9006 exhibits broad spectrum oral antitumor activity and targets the RAF/MEK/ERK pathway and receptor tyrosine kinases involved in tumor progression and angiogenesis. *Cancer Res.* **2004**, *64*, 7099–7109.

(10) Bain, J.; Plater, L.; Elliott, M.; Shpiro, N.; Hastie, C. J.; McLauchlan, H.; Klevernic, I.; Arthur, J. S.; Alessi, D. R.; Cohen, P. The selectivity of protein kinase inhibitors: a further update. *Biochem. J.* **2007**, *408*, 297–315.

(11) Roberts, P. J.; Der, C. J. Targeting the Raf-MEK-ERK mitogen-activated protein kinase cascade for the treatment of cancer. *Oncogene* **2007**, *26*, 3291–3310.

(12) Li, N.; Batt, D.; Warmuth, M. B-Raf kinase inhibitors for cancer treatment. *Curr. Opin. Invest. Drugs* **2007**, *8*, 452–456.

inactive B-RAF forms can contribute to better understanding of the molecular basis of the ligand selectivity. In this way the design of new and selective inhibitors of the active B-RAF forms can also be aided.

Thus, the identification of the binding mode, mechanism of action and selectivity of different B-RAF inhibitors is a challenge and the *in silico* approaches can significantly contribute to their elucidation. Recently, a new series of potent inhibitors based on a disubstituted pyrazine scaffold have been suggested as a starting point for future optimization.[9] In the present study we rely on this series and apply a combination of docking, MD, free energy MM-PBSA[10] and LBE[11] analysis to study the interactions contributing to the B-RAF inhibition, selectivity and conformational stability. We identified a unique salt bridge network, formed mainly by the catalytic residues, in the unbounded B-RAF$^{WT}$ that is destroyed upon ligand binding, proposing a molecular basis of the inactive B-RAF inhibition. Our results suggest that the reorganization of the interactions between Lys483, Glu501, Asp594 and Lys601 are crucial for the ligand selectivity in the inactive B-RAF forms, and for the conformational stability and activity of the protein−ligand complexes. The binding energies of the ligands in the inactive the B-RAF$^{WT}$ correlated well with B-RAF$^{V600E}$ activity, which is in agreement with the low mutant selectivity observed for numerous inhibitors. The results revealed the important role of Lys601 for ligand activity, selectivity and protein stabilization, proposing an explanation of the observed strong kinase activation for the K601E mutated form.

## 2. Methods

**2.1. Data Set.** A data set of 26 inhibitors based on a disubstituted pyrazine scaffold and their B-RAF$^{V600E}$ inhibition activities were taken from the literature.[13] The observed $IC_{50}$ values were converted to logarithmic units: $pIC_{50} = -\log (IC_{50})$. The 3D molecular structures of all 26 compounds were built with the HyperChem software[16] and minimized with the semiempirical AM1[17] method to convergence criterion of 0.01 kcal mol$^{-1}$ Å$^{-1}$.

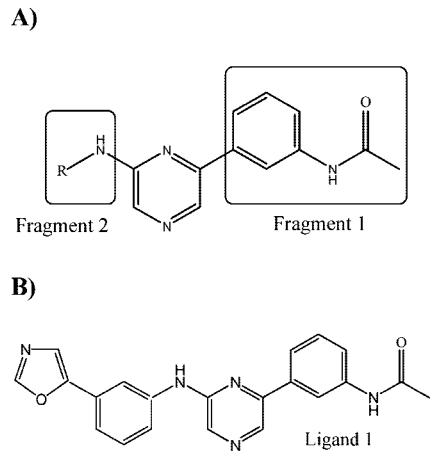


***Figure 1.*** (A) Common structural skeleton of the studied series inhibitors based on a disubstituted pyrazine scaffold. (B) Structure of one of the most active inhibitors, ligand 1.

The data set was randomly divided into a training and a test set of 18 and 8 compounds, respectively. Table 1S in the Supporting Information represents the structures and activity data of the inhibitors studied. Figure 1 illustrates the common structural skeleton of the series and the structure of one of the most active compounds, ligand 1 (see Table 1S in the Supporting Information), which was subject to a detailed MD and free energy analysis.

**2.2. Preparation of the Protein Structures.** The atomic coordinates of the recently obtained crystal structures for B-RAF$^{WT}$, B-RAF$^{V600E}$ and B-RAF-A were retrieved from the protein data bank[18] (pdb codes: 1uwh, 1uwj and 2fb8), and the inhibitors Sorafenib (B-RAF$^{WT}$, B-RAF$^{V600E}$) and SB-590885 (B-RAF-A) were removed while keeping the crystal waters. The regions encompassing residues 601−612 in B-RAF$^{WT}$, 603−614 in B-RAF$^{V600E}$ and 601−613 in B-RAF-A, not solved in the crystal structures, were modeled using the loop building routine in Modeler.[19] The Refine-Loop method was employed to generate their atomic coordinates. In the Refine-Loop method, 500 initially randomized models were created first, and then optimized by extensive MD and simulated annealing procedures in a solution environment.[20−22] The model that had the best

(13) Niculescu-Duvaz, I.; Roman, E.; Whittaker, S. R.; Friedlos, F.; Kirk, R.; Scanlon, I. J.; Davies, L. C.; Niculescu-Duvaz, D.; Marais, R.; Springer, C. J. Novel Inhibitors of B-RAF Based on a Disubstituted Pyrazine Scaffold. Generation of a Nanomolar Lead. *J. Med. Chem.* **2006**, *49*, 407–416.

(14) Kollman, P. A.; Massova, I.; Reyes, C.; Kuhn, B.; Huo, S.; Chong, L.; Lee, M.; Duan, Y.; Wang, W.; Donini, O.; Cieplak, P.; Srinivasan, J.; Case, D.; Cheatham, T. E., III. Calculating structures and free energies of complex molecules: combining molecular mechanics and continuum models. *Acc. Chem. Res.* **2000**, *33*, 889–897.

(15) Fratev, F.; Benfenati, E. 3D-QSAR and molecular mechanics study for the differences in the azole activity against yeastlike and filamentous fungi and their relation to P450DM inhibition. 1. 3-substituted-4(3H)-quinazolinones. *J. Chem. Inf. Model.* **2005**, *45*, 634–644.

(16) HyperChem, Hypercube, Inc., 1115 NW 4th Street, Gainesville, FL 32601, USA.

(17) Dewar, M. J. S.; Zoebisch, E. G.; Healy, E. F.; Stewart, J. J. P. AM1: A New General Purpose Quantum Mechanical Molecular model. *J. Am. Chem. Soc.* **1985**, *107*, 3902–3909.

(18) Berman, H. M.; Westbrook, J.; Feng, Z.; Gilliland, G.; Bhat, T. N.; Weissig, H.; Shindyalov, I. N.; Bourne, P. E. The Protein Data Bank. *Nucleic Acids Res.* **2000**, *28*, 235–242.

(19) Marti-Renom, M. A.; Stuart, A.; Fiser, A.; Sánchez, R.; Melo, F.; Sali, A. Comparative protein structure modeling of genes and genomes. *Annu. Rev. Biophys. Biomol. Struct.* **2000**, *29*, 291–325.

(20) Šali, A.; Blundell, T. L. Definition of general topological equivalence in protein structures: a procedure involving comparison of properties and relationships through simulated annealing and dynamic programming. *J. Mol. Biol.* **1990**, *212*, 403–428.

objective function value[23] and the lowest energy value was selected as the object structure. The resulting A-loop regions of each model were then energy minimized to a convergence criterion of 0.01 kcal mol$^{-1}$ Å$^{-1}$ using the Amber 99 force field[24] as implemented in the HyperChem software in order to remove bad contacts.

**2.3. Molecular Docking.** Molegro Virtual Docker (MVD 2007) was used for the docking analysis.[25] The compounds were docked to B-RAF$^{WT}$, B-RAF$^{V600E}$ and B-RAF-A using the protein structures, prepared as described above. The water molecules were removed during the docking calculations. The binding sites were defined as a 15 Å sphere with a center of coordinates identical to those of the inhibitor in the corresponding crystal structure. During the docking experiments, the ligands were treated as flexible whereas the proteins were rigid. A MolDock-Score (Grid) score function was applied in the analysis and the grid resolution was set to 0.3 Å.[26] MolDock SE (simplex evolution) was used as a search algorithm.[26] The maximum population size and interactions were set to 100 and 1500, respectively. For each ligand 50 independent docking runs were carried out. The lowest energy docking poses, which for the most of the ligands coincided with the most frequent docking solution, were chosen for the analysis presented below.

**2.4. Molecular Dynamics.** In order to obtain a detailed understanding of the binding properties and the structural evolution of the unbounded proteins, a series of 10 ns MD simulations were done for each kinase type in a complex with one the of most potent inhibitors in the series, ligand 1 (see Table 1S in the Supporting Information), and for the unbounded B-RAF$^{WT}$ and B-RAF$^{V600E}$. The unbounded B-RAF forms and the complexes with ligand 1 were prepared with the Amber 9 software,[27] and the MD simulations were performed using NAMD v.2.6.[28] All simulation systems were placed in the center of a cubic simulation box filled with water molecules, represented by the SPC/E water model.[29] Negatively charged chlorine atoms were added to counterbalance the net charges of the proteins. This was done to neutralize the proteins both in their unbounded states and in the complexes. A neutral system is required to use the particle-mesh Ewald (PME) method during MD simulation.[30] The Amber 99 force field was used, along with the General Amber (GAFF) force field to provide any necessary force-field parameters for the ligand.[24,31] The atomic charges of ligand 1 were calculated with the AM1-BCC method.[32] First only the waters and ions were minimized for 2000 steps keeping the proteins fixed. A second minimization was then performed on the whole system for 8000 steps by a conjugate gradient method to a convergence criterion of 0.5 kcal mol$^{-1}$ Å$^{-1}$. Initially, the simulation systems were gradually heated from 0 to 300 K for 50 ps (NTV), then equilibrated for 200 ps and finally production runs of 10 ns (NTP) were submitted. Langevin dynamics was utilized to keep a constant temperature. The Langevin damping coefficient was set to 5 ps$^{-1}$. Constant pressure of 1 atm was imposed using the hybrid Nosé−Hoover Langevin piston method with a decay period of 200 fs and a damping time-scale of 50 fs. The nonbonded cutoff was set to 9.0 Å and the SHAKE algorithm[33] was applied for all bonds involving hydrogen atoms. A 2 fs time step was used, and long-range electrostatic interactions were treated with the PME method.[30] Data were collected every 1 ps during the MD runs.

In order to asses the van der Waals and electrostatic contribution to the ligand 1 binding, the interaction energies between ligand 1 and several residues and protein substructures were calculated by NAMD. To obtain detailed understanding of the conformational stability of the inactive kinases, several interaction energies between key substructures and residues in the unbounded proteins were calculated. These are the A-loop (residues 593−623), the αC-helix (residues 492−506), the P-loop (residues 462−471), Lys601, Glu600 (in B-RAF$^{V600E}$) and the Asp594-Lys601, Lys483-

(21) Šali, A.; Blundell, T. L. Comparative protein modeling by satisfaction of spatial restraints. *J. Mol. Biol.* **1993**, *234*, 779–815.

(22) Melo, F.; Feytmans, E. Novel knowledge-based mean force potential at the atomic level. *J. Mol. Biol.* **1997**, *267*, 207–222.

(23) Šali, A.; Overington, J. P. Derivation of rules for comparative protein modeling from a database of protein structure alignments. *Protein Sci.* **1994**, *3*, 1582–1596.

(24) Cornell, W. D.; Cieplak, P.; Bayey, C. I.; Gould, I.; Merz, K. M.; Ferguson, D. M.; Spellmeyr, D.; Fox, T.; Caldmell, J. W.; Kollman, P. A Second Generation Force Field for the Simulation of Proteins, Nucleic Acids, and Organic Molecules. *J. Am. Chem. Soc.* **1995**, *117*, 5179–5197.

(25) Molegro Virtual Docker (MVD 2007), Molegro ApS, Hoegh-Guldbergs Gade 10, Building 1090, DK-8000 Aarhus C, Denmark.

(26) Thomsen, R.; Christensen, M. H. MolDock: A New Technique for High-Accuracy Molecular Docking. *J. Med. Chem.* **2006**, *49*, 3315–3321.

(27) Case, D. A.; Darden, T. A.; Cheatham, T. E., III; Simmerling, C. L.; Wang, J.; Duke, R. E.; Luo, R.; Merz, K. M.; Pearlman, D. A.; Crowley, M.; Walker, R. C.; Zhang, W.; Wang, B.; Hayik, S.; Roitberg, A.; Seabra, G.; Wong, K. F.; Paesani, F.; Wu, X.; Brozell, S.; Tsui, V.; Gohlke, H.; Yang, L.; Tan, C.; Mongan, J.; Hornak, V.; Cui, G.; Beroza, P.; Mathews, D. H.; Schafmeister, C.; Ross, W. S.; Kollman, P. A. *AMBER 9*; University of California: San Francisco, 2006.

(28) James, C. P.; Braun, R.; Wang, W.; Gumbart, J.; Tajkhorshid, E.; Villa, E.; Chipot, C.; Skeel, R. D.; Kale, L.; Schulten, K. Scalable molecular dynamics with NAMD. *J. Comput. Chem.* **2005**, *26*, 1781–1802.

(29) Berendsen, H. J.; Grigera, J.; Straatsma, T. The missing term in effective pair potentials. *J. Phys. Chem.* **1987**, *91*, 6269–6271.

(30) Darden, T.; York, D.; Pederson, L. Particle mesh Ewald: an N.log(N) method for Ewald sums in large systems. *J. Chem. Phys.* **1993**, *98*, 10089–10092.

(31) Wang, J.; Wolf, R. M.; Caldwell, J. W.; Kollman, P. A.; Case, D. A. Development and testing of a general AMBER force field. *J. Comput. Chem.* **2004**, *25*, 1157–1174.

(32) Jakalian, A.; Bush, B. L.; Jack, B. D.; Bayly, C. I. Fast, Efficient Generation of High-Quality Atomic Charges. AM1-BCC Model: I. Method. *J. Comput. Chem.* **2000**, *21*, 132–146.

(33) Ryckaert, J. P.; Ciccotti, G.; Berendsen, H. J. C. Numerical integration of the Cartesian equations of motion of a system with constraints: Molecular dynamics of *n*-alkanes. *J. Comput. Phys.* **1977**, *23*, 327–341.

Glu501 and Asn581-Asp576 ion pairs. The average energies in both the complexes and the unbounded proteins were calculated for the time interval 7−10 ns, when good convergence was reached. The average hydrogen bond distances and the corresponding standard deviations were calculated for the time interval 3−10 ns with the VEGA software.[34] Visualization of the proteins and the protein−ligand complexes was carried out with the VMD package.[35]

**2.5. MM-PBSA Calculations.** The binding free energies of all the systems were analyzed using the MM-PBSA (molecular mechanics Poisson−Boltzmann/surface area) approach.[10] The binding free energies ($\Delta G_{bind}$) were computed as

$$\Delta G_{bind} = G_{complex} - (G_{protein} + G_{ligand}) \quad (1)$$

$$\Delta G_{bind} = \Delta G_{gas} + \Delta G_{solv} - T\Delta S \quad (2)$$

$$\Delta G_{gas} = \Delta G_{ele} + \Delta G_{vdW} \quad (3)$$

$$\Delta G_{solv} = \Delta G_{PB} + \Delta G_{nonpolar} \quad (4)$$

$$\Delta G_{nonpolar} = \gamma A + b \quad (5)$$

The sum of the molecular mechanical free energies, $\Delta G_{gas}$, is divided into contributions from the electrostatic potential ($\Delta G_{ele}$) and the van der Waals ($\Delta G_{vdW}$) potential. The solvation free energy ($\Delta G_{solv}$) is composed of two parts, the polar solvation free energy ($\Delta G_{PB}$) and the nonpolar solvation free energy ($\Delta G_{nonpolar}$). All the energies are averaged along the MD trajectories. The snapshots of each system were sampled from the last 4 ns single trajectory with an interval of 10 ps, i.e. 400 snapshots. The single trajectory approach was applied to estimate the energies, as estimation of energies in this manner has proven successful in many studies.[36,37] A part of the reason for the success of this approach is the cancelation of errors that hides the effect of incomplete sampling. $\Delta G_{gas}$ was obtained using the Amber 9 sander module, and estimation of $\Delta G_{PB}$ was conducted with a built-in module, PBSA in Amber 9. $\Delta G_{nopolar}$ was determined from eq 5, where $A$ is the solvent-accessible surface area estimated using the Molsurf program, which is part of the Amber 9 suite, with a solvent probe radius of 1.4 Å. $\gamma$ and $b$ are empirical constants set to 0.00542 kcal mol$^{-1}$ Å$^{-2}$ and 0.92 kcal mol$^{-1}$, respectively. We estimated the conformational entropy contributions (translation, rotation, and vibration) to the binding free energy using normal-mode analysis, which was carried out using the Nmode program in Amber.[27] Prior to the normal-mode calculations, the complex, the receptor, and ligand 1 were energy minimized with a distance-dependent dielectric constant $\varepsilon = 4r$ and convergence tolerance tighter than rmsd = $10^{-4}$ kcal mol$^{-1}$ Å$^{-1}$. Fifty normal-mode calculations were performed.

**2.6. Evaluation of the Total and Local Binding Energies for LBE Analysis.** In order to calculate the binding energies for the substructures within the inhibitors, the LBE approach was used. The LBE method estimates the binding energies between structural fragments or substituents within the ligand and the surrounding protein residues, and uses them as descriptors in an QSAR analysis. Thus, information about interacting hot spots within the binding pocket can be obtained and their relative contribution and relationship to the inhibition activity can be estimated.[38,39]

After the docking procedure was completed, an energy minimization of 5000 steps and 600 ps MD simulation within 18 Å of the ligand center was carried out for each complex. All atoms outside this sphere were kept frozen during the MD runs. The complexes were prepared with the Amber 9 package. The MD simulations were carried out with the NAMD 2.6 software. The Amber 99 and the GAFF force fields were employed for the proteins and ligands, respectively. After the MD simulation was completed, all the complexes were minimized again for up to 5000 steps to convergence criterion of 0.1 kcal mol$^{-1}$ Å$^{-1}$. The total binding energy of each ligand was calculated using the following equation:

$$E_{binding} = E_{complex} - (E_{ligand} + E_{receptor}) \quad (6)$$

where $E_{ligand}$, $E_{receptor}$ and $E_{complex}$ are the energies of the ligand, the protein and their complex, respectively. The van der Waals (vdW) and the electrostatic contributions to the total binding energies were obtained by eq 6 using the corresponding energy terms.

LBEs of the selected molecular substructures and substituents were calculated by the following approximation:

$$\mathrm{LBE} = E_{bound} - E_{unbound} \quad (7)$$

where $E_{bound}$ and $E_{unbound}$ are the energies of the substituent in a complex with the protein and in the unbound ligand, respectively. A LBE is thus the difference between the van der Waals and electrostatic energies of a substituent in the presence of the protein and the corresponding energies of the same substituent within the unbound ligand. All the LBE calculations were performed with the HyperChem software using the Amber 99 force field as implemented in this package, and using the same atomic charges for the ligands as in the MD simulations. After the MD simulation was completed, each complex was energy minimized, and the corresponding ligands were also minimized in their unbound state. The LBEs of the substituents were then calculated by

(34) Pedretti, A.; Villa, L.; Vistoli, G. VEGA: a versatile program to convert, handle and visualize molecular structure on Windows-based PCs. *J. Mol. Graphics Modell.* **2002**, *21*, 47–49.

(35) Humphrey, W.; Dalke, A.; Schulten, K. VMD - Visual Molecular Dynamics. *J. Mol. Graphics Modell.* **1996**, *14*, 33–38.

(36) Li, L.; Uversky, V. N.; Dunker, A. K.; Meroueh, S. O. A computational investigation of allostery in the catabolite activator protein. *J. Am. Chem. Soc.* **2007**, *129*, 15668–15676.

(37) Stoica, I.; Sadiq, S. K.; Coveney, P. V. Rapid and Accurate Prediction of Binding Free Energies for Saquinavir-Bound HIV-1 Proteases. *J. Am. Chem. Soc.* **2008**, *130*, 2639–2648.

(38) Fratev, F.; Lo Piparo, E.; Benfenati, E.; Mihaylova, E. Toxicity study of allelochemical-like pesticides by a combination of 3D-QSAR, docking, Local Binding Energy (LBE) and GRID approaches. *SAR QSAR Environ. Res.* **2007**, *18*, 675–692.

(39) Fratev, F.; Benfenati, E. A Combination of 3D-QSAR, Docking, Local binding energy (LBE) and GRID Study of the Species Differences in the Carcinogenicity of Benzene Derivatives Chemicals. *J. Mol. Graphics Modell.* **2008**, *27*, 147–160.

eq 7. It should be noted that the LBE method considers only the van der Waals and electrostatic energies similarly to the initial and often used version of the Comparative Binding Energy (COMBINE) approach.[40] While the COMBINE method is useful to identify the protein residues which are significant for ligand binding, molecular substituents of key importance to ligand binding are studied with the LBE method. It has been shown that both the COMBINE and the LBE methods have shown useful applications in several studies.[15,38,39,41−43]

**2.7. Statistical Analysis.** Statistical analysis was performed by the multiple linear regression (MLR) method as implemented in Molegro Data Modeler (MDM).[44] The quality of the MLR models was assessed by the correlation coefficient ($r^2$), the cross-validated correlation coefficient using the leave-one-out method ($q^2$), the root-mean-square error (RMSE) and the Fisher's criterion ($F$). The standard error for each of the regression constants is shown in parentheses in the QSAR equations. The quality of the MLR test set results was evaluated with the correlation coefficient ($r^2_{pred}$) and the root-mean-square error ($RMSE_{pred}$) of the predictions.

## 3. Results

**3.1. Docking Results.** All the 26 inhibitors were docked to the protein structures of the inactive wild type and the mutant forms of the kinase, B-RAF$^{WT}$, B-RAF$^{V600E}$, and to the active V600E form, B-RAF-A, as well. The obtained docking scores for the generated poses were significantly lower in B-RAF$^{WT}$ and B-RAF$^{V600E}$ than in B-RAF-A (data not shown, for ligand 1 see Table 1). Thus, the docking results indicate that the compounds can bind to the inactive B-RAF. The ligands are buried deeply between the N and C lobes and exhibit similar binding mode as the well-known inhibitor sorafenib. Sorafenib binds with an identical mode to both the inactive forms, B-RAF$^{WT}$ and B-RAF$^{V600E}$, and inhibits the wild type stronger than the mutant form.[9]

Figures 1S and 2S in the Supporting Information present docking views of ligand 1 in the binding sites of B-RAF$^{WT}$ and B-RAF$^{V600E}$, respectively. In B-RAF$^{WT}$, the phenyl ring common for all inhibitors in the series and the attached

***Table 1.*** The Calculated Docking Scores and Average Interaction Energies (kcal/mol) between Ligand 1 and the Protein, Ligand 1 and Specific Residues within the Protein and Key Substructures in the Binding Site of the Studied B-RAF Types[a]

| | B-RAF$^{WT}$ | | | B-RAF$^{V600E}$ | | | B-RAF-A | | |
|---|---|---|---|---|---|---|---|---|---|
| | vdW | elect. | total | vdW | elect. | total | vdW | elect. | total |
| Complexes | | | | | | | | | |
| docking score[b] | | | −179.1 | | | −166.2 | | | −151.7 |
| ligand−protein[c] | −47.5 ± 2.5 | −29.1 ± 4 | −76.6 ± 4.4 | −42 ± 2.6 | −29.7 ± 5.1 | −71.7 ± 5.4 | −40.9 ± 2.5 | −22.1 ± 2.8 | −63.0 ± 3.5 |
| ligand−WAT[d] | −0.5 ± 1.3 | −10.1 ± 3.4 | −10.6 ± 3.0 | −3.1 ± 1.5 | −8.5 ± 5.0 | −11.6 ± 4.5 | −3.9 ± 1.8 | −11.6 ± 4 | −15.5 ± 3.8 |
| ligand−E501−K601[e] | −6.4 ± 1.5 | −24.7 ± 3 | −31.1 ± 2.5 | −5.5 ± 1.3 | −17.0 ± 7.7 | −22.5 ± 7.3 | na[h] | na | na |
| ligand−K601[f] | −1.5 ± 0.5 | −24.4 ± 2.6 | −25.9 ± 1.9 | −1.0 ± 0.6 | −16.1 ± 7.1 | −17.1 ± 6.8 | na | na | na |
| A-loop−protein[g] | −73.1 ± 4.6 | −191.0 ± 14 | −264.2 ± 14.6 | −53.7 ± 5.0 | −98.0 ± 16.7 | −151.7 ± 17.6 | −101.8 ± 5.4 | −246.9 ± 19.2 | −348.7 ± 19.1 |
| Unbounded Kinases | | | | | | | | | |
| A-loop−protein[i] | −112.1 ± 7.0 | −190.3 ± 13.6 | −302.4 ± 12.6 | −106.2 ± 5.6 | −120.6 ± 12.2 | −226.8 ± 12.3 | na | na | na |
| A-loop−C-helix[j] | −17.5 ± 3.7 | −42.1 ± 7.7 | −59.7 ± 7.3 | −26.9 ± 3.2 | −5.8 ± 5.4 | −35.3 ± 5.1 | na | na | na |
| A-loop−P-loop[k] | −12.7 ± 2.2 | −18.2 ± 5.5 | −30.9 ± 5.1 | −22.6 ± 2.0 | −11.9 ± 2.8 | −34.4 ± 3.2 | na | na | na |

[a] The van der Waals and the electrostatic contribution to the total interactions energies are listed along with the measured standard deviations. [b] MolDock score values for ligand 1. [c] Ligand−protein interactions. [d] Ligand−water interactions. [e] Interactions between ligand 1, Lys601 and Glu501. [f] Interactions between ligand 1 and Lys601. [g] A-loop (residues 593−623) interactions with the remaining protein residues. [h] Not available. [i] The interactions between the A-loop and the remaining protein. [j] The interactions between the A-loop and the αC-helix (residues 492−506). [k] The interactions between the A-loop and the P-loop (residues 462−471).

(40) Ortiz, A. R.; Pisabarro, M. T.; Gago, F.; Wade, R. C. Prediction of Drug Binding Affinities by Comparative Binding Energy Analysis. *J. Med. Chem.* **1995**, *38*, 2681–2691.

(41) Pastor, M.; Gago, F.; Cruciani, G. Comparative Binding Energy (COMBINE) Analysis on a series of Glycogen Phosphorylase Inhibitors. Comparison with GRID/GOLPE Models. In *Molecular Modeling and Prediction of Bioactivity*; Gundertofte, K., Jorgensen, F. S., Eds.; Kluwer: New York, 2000; pp 329−330.

(42) Wade, R. C.; Oritz, A. R.; Gago, F. Comparative binding energy analysis. *Perspect. Drug Discovery Des.* **1998**, *9*, 19–34.

(43) Wang, T.; Wade, R. C. Comparative binding energy (COMBINE) analysis of influenza neuraminidase-inhibitor complexes. *J. Med. Chem.* **2001**, *44*, 961–671.

(44) Molegro Data Modeller (MDM, version 1.1.0), Molegro ApS, Hoegh-Guldbergs Gade 10, Building 1090, DK-8000 Aarhus C, Denmark.

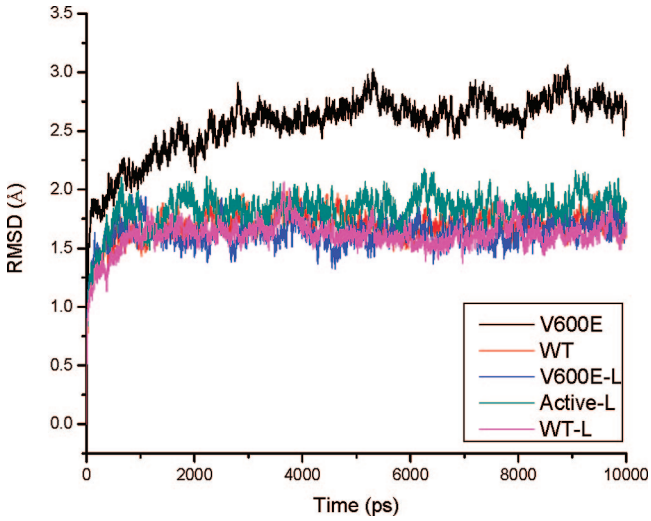


***Figure 2.*** The rmsd of the protein backbone atoms (C, Cα and N atoms) of the unbounded B-RAF$^{WT}$ (WT) and B-RAF$^{V600E}$ (V600E) along with the complexes of ligand 1 with B-RAF$^{WT}$ (WT-L), B-RAF$^{V600E}$ (V600E-L) and B-RAF-A (Active-L).

substituents (fragment 1, see Figure 1) were surrounded by Lys601, Glu501, Val504, Asp594, Ser602, His574 and Ile592, whereas the remaining part of the ligand structure was in close contact with Gly593, Leu505, Lys483, Ile527, Thr529, Leu514 and Phe595. In B-RAF$^{V600E}$ a similar binding mode and similar contacts with the residues were observed. It was seen that all 26 inhibitors formed hydrogen bonds with Lys601 and Glu501 in both the wild type and the mutant form. The only difference is due to the change of the A-loop conformation leading to a ligand interaction with Ser602 instead of Ser607 in B-RAF$^{WT}$.

Based on the initial results two different analyses were done. First, a detailed MD analysis of all the B-RAF complexes was performed and the binding free energies were calculated with the MM-PBSA approach to investigate the binding mode and selectivity of ligand 1. The interactions between the kinase structural elements of the unbounded proteins and the mechanism of B-RAF$^{V600E}$ activation were also analyzed by a set of MD simulations. Second, based on the similar binding mode identified for the ligands in B-RAF$^{WT}$ and B-RAF$^{V600E}$, it is reasonable to suggest that the same ligand−kinase interactions will lead to similar effect. Thus, we searched further for potential relationships between B-RAF$^{WT}$ ligand−protein interactions and B-RAF$^{V600E}$ activity to specify the main factors for the inhibitors selectivity. The key substituents and substructure fragments involved in ligand binding were analyzed based on a LBE approach.

**3.2. Molecular Dynamics and Estimation of the Binding Free Energies. 3.2.1 Overall MD Analysis.** To obtain more accurate information on the binding mode and ligand−protein interactions, a series of five 10 ns MD simulations were carried out. Figure 2 shows the root-mean-square deviations (rmsd) of the protein backbone atoms of B-RAF$^{WT}$, B-RAF$^{V600E}$ and B-RAF-A in a complex with ligand 1, and of the unbounded B-RAF$^{WT}$ and B-RAF$^{V600E}$, respectively. For each complex the lowest energy docking pose of ligand 1 was used as the initial structure.

Interestingly, the unbound wild type kinase and all the complexes have similar rmsd values and reached equilibrium after 1.5 ns simulation time, while the corresponding rmsd for the unbound V600E mutant form is significantly larger and it took 3.5 ns to reach equilibrium (see Figure 2). The rmsd of the backbone B-RAF$^{WT}$, B-RAF$^{V600E}$ and B-RAF-A atoms, in a complex with ligand 1, were 1.61 Å (SD = 0.12), 1.63 Å (SD = 0.11) and 1.83 Å (SD = 0.15), respectively, whereas for unbounded proteins we obtained rmsd values of 1.69 Å (SD = 0.12) for B-RAF$^{WT}$ and 2.56 Å (SD = 0.26) for B-RAF$^{V600E}$.

Table 1 summarizes the calculated docking scores as well as the ligand−protein and the residue average interaction energies of ligand 1 in the binding sites of the studied B-RAF types. Inspection of the energy values in Table 1 reveals that interaction between only one residue, Lys601, and ligand 1 accounts for a significant part of the ligand−protein interaction energy for the inactive forms, with a particularly strong electrostatic component. The interaction energy terms are similar for the wild type and the mutant complexes, with the exception of the interaction energy between the flexible A-loop and the remaining protein. This term decreases strongly upon ligand binding for both the inactive forms.

**3.2.2. Free Energy Calculations.** To obtain information about the selectivity of ligand 1 for the studied B-RAF types, the binding free energies of this inhibitor were calculated with the MM-PBSA method. Table 2 presents the estimated free binding energies along with the contribution of the individual energy terms. The calculations show that ligand 1 can only bind to the inactive B-RAF$^{WT}$ and B-RAF$^{V600E}$ with higher selectivity to the wild type. The free energy of ligand 1 in a complex with B-RAF-A is positive, demonstrating that ligand 1 cannot bind to the active form. The same is presumably the case for the other ligands in the series, as they are highly structurally similar to ligand 1. The obtained free energy of ligand 1 in V600E mutant is in good agreement with the experimental value of −8.25 kcal/mol[13] (see Table 1S in the Supporting Information). Indeed, the $\Delta G$ calculated by the approximation $\Delta G \approx RT \ln IC_{50}$ could be used only for making a rough estimation of the free energy since the $IC_{50}$ has been shown to correlate with the constant of inhibition ($K_i$) for similar and smaller inhibitors.[45−48]

(45) Tute, M. S. Drug design: The present and the future. *Adv. Drug Res.* **1995**, *26*, 48–50.
(46) Brandt, R. B.; laux, J. E.; Yates, S. W. Calculation of inhibitor $K_i$ and inhibitor type from the concentration of inhibitor for 50% inhibition for Michaelis-Menten enzymes. *Biochem. Med. Metab. Biol.* **1987**, *37*, 344–349.
(47) Price, M. L. P.; Jorgensen, W. L. Analysis of binding affinities for celecoxib analogues with COX-1 and COX-2 from combined docking and Monte Carlo simulations and insight into the COX-2/COX-1 selectivity. *J. Am. Chem. Soc.* **2000**, *122*, 9455–9466.

***Table 2.*** The Binding Free Energies (kcal/mol) of Ligand 1 Calculated with the MM-PBSA Method

| B-RAF[a] | $\Delta G_{vdW}$[b] | $\Delta G_{elect.}$[b] | $\Delta G_{sol}$[b] | $T\Delta S$[b] | $\Delta G_{total}$[b] |
|---|---|---|---|---|---|
| B-RAF$^{WT}$ | –45.74 (0.7) | –21.63 (0.4) | 38.72 (0.5) | –19.72 (1.4) | –8.93 (1.6) |
| B-RAF$^{V600E}$ | –42.33 (0.8) | –25.66 (0.5) | 42.68 (0.4) | –17.95 (1.5) | –7.36 (1.5) |
| B-RAF-A | –50.79 (0.6) | –4.95 (0.3) | 51.97 (0.3) | –17.49 (1.3) | 13.72 (1.4) |

[a] The B-RAF form. [b] $\Delta G_{vdW}$, $\Delta G_{elect}$, $\Delta G_{sol}$ and $T\Delta S$ are the contributions of the van der Waals, the electrostatic, the solvation energies and the entropy changes to the total free energy of binding ($\Delta G_{total}$).

By taking a closer look at the individual energy contributions in Table 2, it is clearly seen that the small electrostatic contribution for ligand 1 in B-RAF-A tilts the balance toward a positive overall free energy of binding. As mentioned above, the ligand is integrated into a strong salt bridge network when it binds to the wild type and the mutant forms, rendering a strong electrostatic contribution.

The wild type complex is slightly more stable than the mutant complex, with the van der Waals and the solvation energy contribution favoring the wild type form and the electrostatic contribution and the entropy term favoring the mutant form. The solvation energy is more positive in the V600E mutant and the active form indicating that the ligands were better exposed to water interactions in these complexes. These results agree with the ligand−water interaction energies listed in Table 1.

Based on the MM-PBSA results, a detailed analysis was performed of the B-RAF$^{WT}$ and B-RAF$^{V600E}$ kinases in their unbounded form and in complex with ligand 1.

**3.2.3. Molecular Dynamics of Unbounded B-RAF$^{WT}$ and in Complex with Ligand 1.** Figure 3A shows the B-RAF$^{WT}$ conformation in a complex with ligand 1 after 10 ns MD simulation. Figure 3B presents a close view of the compound within the binding site. Ligand 1 was integrated into the salt bridge network with Glu501-Lys601-Asp594 in which Lys601 plays a central role by forming strong hydrogen bonds with Glu501 and the carbonyl oxygen within ligand 1. The average distances between Lys601-Glu501 and Lys601-ligand 1 carbonyl oxygen were 2.83 Å ± 0.12 and 2.75 Å ± 0.17, respectively. As the same carbonyl group is present in all the inhibitors, one can speculate that its interaction with the residues in the above-mentioned salt bridge network is of a key importance for the whole series of inhibitors.

Glu501 makes hydrogen bonds with Lys483 and the ligand amino group in fragment 2 with an O···N atom distance of 3.23 Å ± 0.36. The average distance between Lys483 and Asp594 in the complex was 6.13 Å ± 0.33, whereas in the unbounded kinase the corresponding average distance is 4.18 Å ± 1.01. The calculated Lys483−Asp594 interaction energies in the complex and the unbounded B-RAF$^{WT}$ were −34.8 ± 2.9 kcal/mol and −69.1 ± 4.4 kcal/mol, respectively. Presumably, the disruption of the Lys483-Asp594 link

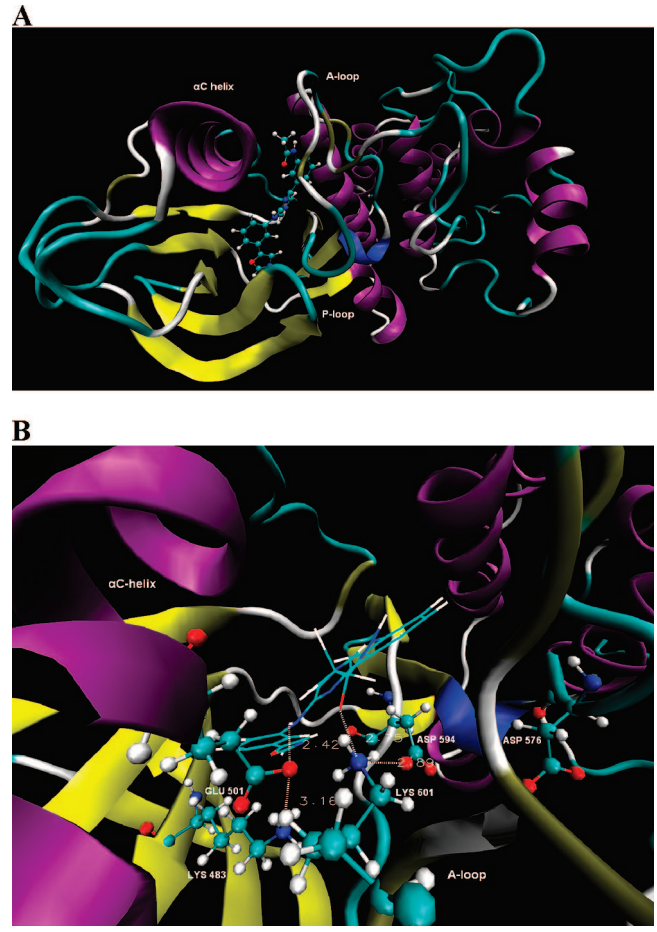


***Figure 3.*** (A) The conformation of B-RAF$^{WT}$ in a complex with ligand 1 after 10 ns of simulation. (B) A close look at the binding mode of ligand 1 in B-RAF$^{WT}$. The dotted lines and the corresponding values present the hydrogen bonds and their distances.

and the resulting conformational changes in the catalytic and ATP coordinating residues are significant for the mechanism of B-RAF$^{WT}$ inhibition for this compound. This finding is supported by the fact that the D594V and the K483M mutations lead to the highest autoinhibition of the kinase.[4] Moreover, due to its binding in this specific cavity ligand 1 occupied the space where the A-loop would be positioned in the active state, thus preventing the activation of B-RAF. An additional support for this finding is that the van der Waals A-loop−protein interaction energy was considerably lower than the corresponding energy in the unbounded kinase (see Table 1). Thus, the ligand simultaneously blocks the phosphorylation of B-RAF$^{WT}$ by reorganization of the interactions in the natural ATP binding site and by restriction of the active segment flexibility. Most likely, this mechanism

(48) Wang, J.; Morin, M.; Wany, W.; Kollman, P. A. Use of MM-PBSA in reproducing the binding free energies to HIV-1 RT of TIBO derivatives and predicting the binding mode to HIV-1 RT of efavirenz by docking and MM-PBSA. *J. Am. Chem. Soc.* **2001**, *123*, 5221–5230.

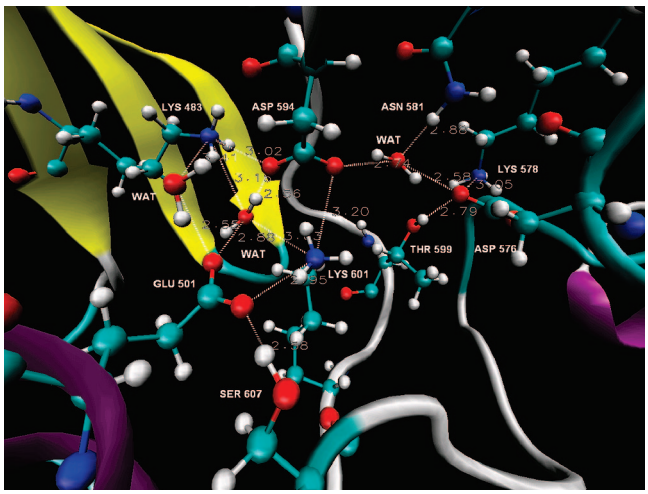


***Figure 4.*** A close look of the identified salt bridge network in the unbounded B-RAF$^{WT}$. The dotted lines and the corresponding values present the hydrogen bonds and their distances.

inhibition of the inactive B-RAF is not unique because a comparable binding mode was found for several other inhibitors.[4,6,49]

According to Table 1 Lys601 and Glu501 gave the main contribution (about 40%) to the total interaction energy (van der Waals plus electrostatic) of the ligand−protein complex. Approximately 85% of the electrostatic interactions come from these residues indicating the critical role of Lys601 and Glu501 in the binding of ligand 1. Moreover, ligand 1−Lys601 interactions comprised 34% of the total ligand−protein interactions and 84% of the electrostatic ones. These data demonstrate that Lys601 has an important role in the B-RAF$^{WT}$ ligand inhibition.

In the unbounded B-RAF$^{WT}$, a water-mediated salt bridge network between Lys483, Glu501, Asp594 and Lys601 was observed and remained stable during the whole simulation. Lys601 was also joined in a second water-mediated hydrogen bond bridge between Asp594, Asn581 and Asp576 forming a unique network, probably important for the wild type protein function and conformation (Figure 4). The average distances of the Lys601-Glu501 and Lys601-Asp594 ion pairs were 2.91 Å ± 0.51 and 2.96 Å ± 0.34, respectively. The corresponding electrostatic interaction energies were −93.8 ± 3.5 kcal/mol and −58.2 ± 2.6 kcal/mol, and thus, the Lys601-Glu501 comprised 47% of the electrostatic A-loop−protein interactions, and 31% of the total ones (see Table 1). It has been established that Lys483 and Asp594 are highly conserved residues and of key importance for the ATP binding and coordination in the kinase family, and in many cases the Lys483−Glu501 interactions increase the phosphorylation potential.[50,51] The strong interactions of Lys601 with these residues and the participation in the salt bridge with Lys483 indicate the important role of the lysine in the B-RAF$^{WT}$ conformational stability, which can explain the observed strong kinase activation in the presence of the K601E mutation. The participation of Asp594 in the identified hydrogen bond network presumes the significance of this residue in the B-RAF wild type protein function and suggests a molecular basis of the D594V mutation.[4] Interestingly, several other residues with known mutations that affect the kinase activity are joined in the identified salt bridge network, or are in neighboring positions to the residues in this network. Asn581 and Thr599 were involved in the hydrogen bond network via direct and water mediated hydrogen bond with both Asp576 and Asp594 (see Figure 4). We observed that Gly596 makes a stable hydrogen bond with Asp594, while the neighboring residues Phe595 and Leu597 interact with Asp594 and Lys483, respectively. It has been shown that the mutations of the Asn581, Thr599, Gly596, Phe595 and Leu597 residues lead to significant increase or decrease in the kinase activity.[4] Presumably, the mutations of the residues of the above-mentioned salt bridge network will alter the electrostatic interactions and subsequently lead to conformational changes of the catalytic residues.

**3.2.4. Molecular Dynamics of B-RAF$^{V600E}$ in a Complex with Ligand 1.** Figures 5A and 5B show the B-RAF$^{V600E}$ conformation in a complex with ligand 1 after 10 ns MD simulation and a close view of the compound binding site, respectively. Ligand 1 binding mode in B-RAF$^{V600E}$ was similar to the wild type. The compounds were well overlapped after the protein alignment, except for the common phenyl ring and attached substituents (see Figure 6). The difference is due to the conformational changes of Lys601, caused by a hydrogen bond with the ligand carbonyl group, similarly to the wild type, with an average distance of 3.01 Å ± 0.41. Most of the ligand−protein interactions in B-RAF$^{WT}$ were present in B-RAF$^{V600E}$ too. Glu501 forms a water mediated hydrogen bond with the ligand amino group with an average distance of 3.43 Å ± 0.53. The larger distance of the latter bond compared with the B-RAF$^{WT}$ complex is caused by a water molecule involved in the Glu501−NH$_{ligand}$ interactions. The interaction of the inhibitor with Lys601 and Glu501 comprised 31% of the total ligand−protein interactions, which supports the finding of the binding to the wild type kinase being the most favorable (see Table 1).

(49) Wolin, R. L.; Bembenek, S. D.; Wei, J.; Crawford, S.; Lundeen, K.; Brunmark, A.; Karlsson, L.; Edwards, J. P.; Blevitt, J. M. Dual Binding Site Inhibitors of B-RAF Kinase. *Bioorg. Med. Chem. Lett.* **2008**, *18*, 2825–2829.

(50) Hanks, S. K.; Hunter, T. Protein kinases 6. The eukaryotic protein kinase superfamily: kinase (catalytic) domain structure and classification. *FASEB J.* **1995**, *9*, 576–596.

(51) Liao, J. J. Molecular recognition of protein kinase binding pockets for design of potent and selective kinase inhibitors. *J. Med. Chem.* **2007**, *50*, 409–424.

(52) Cheung, M.; Sharma, A.; Madhunapantula, S. V.; Robertson, G. P. Akt3 and mutant V600E B-Raf cooperate to promote early melanoma development. *Cancer Res.* **2008**, *68*, 3429–3439.

(53) Grbovic, O. M.; Basso, A. D.; Sawai, A.; Ye, Q.; Friedlander, P.; Solit, D.; Rosen, N. V600E B-Raf requires the Hsp90 chaperone for stability and is degraded in response to Hsp90 inhibitors. *Proc. Natl. Acad. Sci. U.S.A.* **2006**, *103*, 57–62.

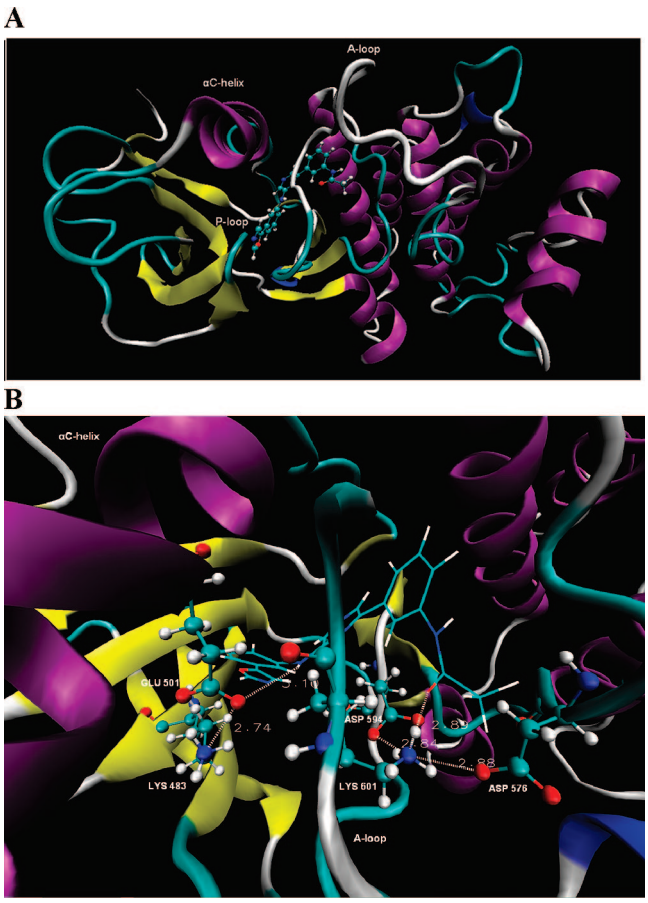


***Figure 5.*** (A) The conformation of B-RAF$^{V600E}$ in a complex with ligand 1 after 10 ns of simulation. (B) A close look of the binding mode of ligand 1 in B-RAF$^{V600E}$. The dotted lines and the corresponding values present the hydrogen bonds and their distances.

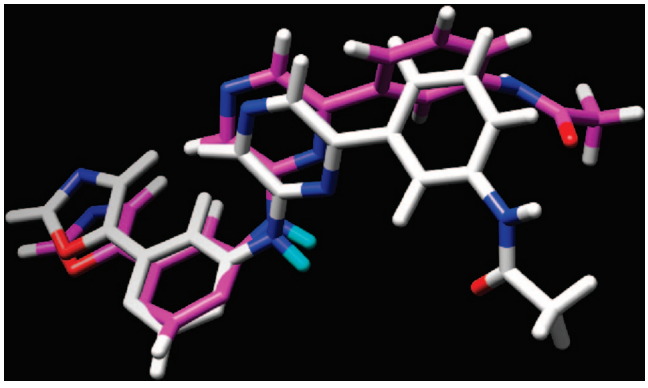

***Figure 6.*** The overlap of ligand 1 in the binding sites of B-RAF$^{WT}$ (white structure) and B-RAF$^{V600E}$ (purple structure) based on the protein alignment.

The A-loop−protein interaction energies were weaker than those in the unbounded protein (see Table 1), which is caused by the A-loop movement restriction toward the $\beta$6-strand, i.e., the pocket where the active segment is positioned in the active state. The inhibitor occupied the space between the A-loop, the $\beta$6-strand and the αC-helix, in a similar way to sorafenib, presumably preventing the transition of the A-loop to its active position or to change the protein to some

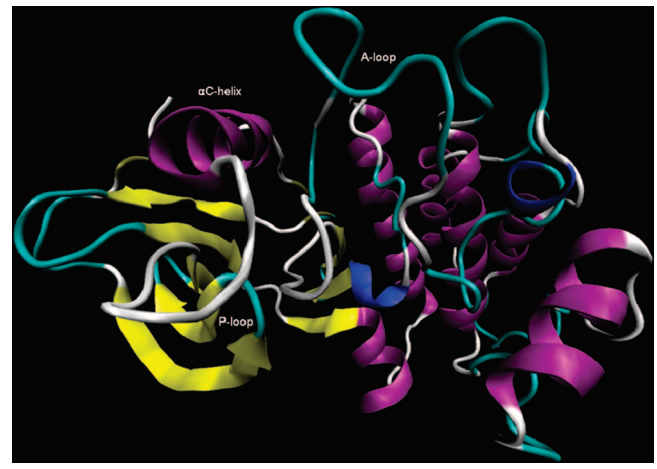


***Figure 7.*** The conformation of the unbounded B-RAF$^{V600E}$ after 10 ns of simulation.

intermediate conformation favorable for the further protein−protein cooperation.[52,53] An additional support for these results is the much higher rmsd observed for the unbounded B-RAF$^{V600E}$ seen in Figure 2. This is discussed further in the following paragraph.

The ligand binding in this specific cavity and the reorganization of the catalytic residues are in our opinion the most likely main mechanisms of the ligand 1−B-RAF$^{V600E}$ inhibition. Thus, ligand 1 has a similar mechanism of action in both wild type and mutant, but binds more strongly to B-RAF$^{WT}$, which is confirmed with the higher wild type selectivity calculated by the MM-PBSA approach. The fact that ligand 1 interacts with residues that were well solved in the crystal structure suggests that the loop modeling of the A-loop fraction not solved in the crystal structure would not be likely to significantly affect the obtained results. Hence, the inhibition mechanism suggested above could be relevant for other possible models of the missing A-loop portion.

**3.2.5. Molecular Dynamics of Unbounded B-RAF$^{V600E}$.** In order to highlight the processes of B-RAF$^{V600E}$ destabilization and to obtain detailed understanding of the initial steps of the mutant activation, a separate run of 10 ns for the unbounded B-RAF$^{V600E}$ was studied. Dramatic changes in the activation segment folding and other protein fragments compared with the B-RAF$^{WT}$ and B-RAF$^{V600E}$ in a complex were observed (see Figures 5A and 7). The initial A-loop model differed from those in the wild type kinase, but also the rmsd value of the active segment backbone atoms significantly increased during the first 6 ns of the simulation to a value of 6 Å (see Figure 3S in the Supporting Information). The A-loop adopted an open conformation similar to the active form of the kinase (see Figure 9A), but the typical shift of the initial portion of the activation loop (residues 598−602) to the $\beta$6-strand in the active state was not seen for the simulation period due to the strong salt bridge network between Asp594, Asp576 and Lys601.

Intriguingly, the A-loop−protein electrostatic interaction energy, which gives a major contribution to the total energy (see Table 1), decreases gradually by ca. 100 kcal/mol during

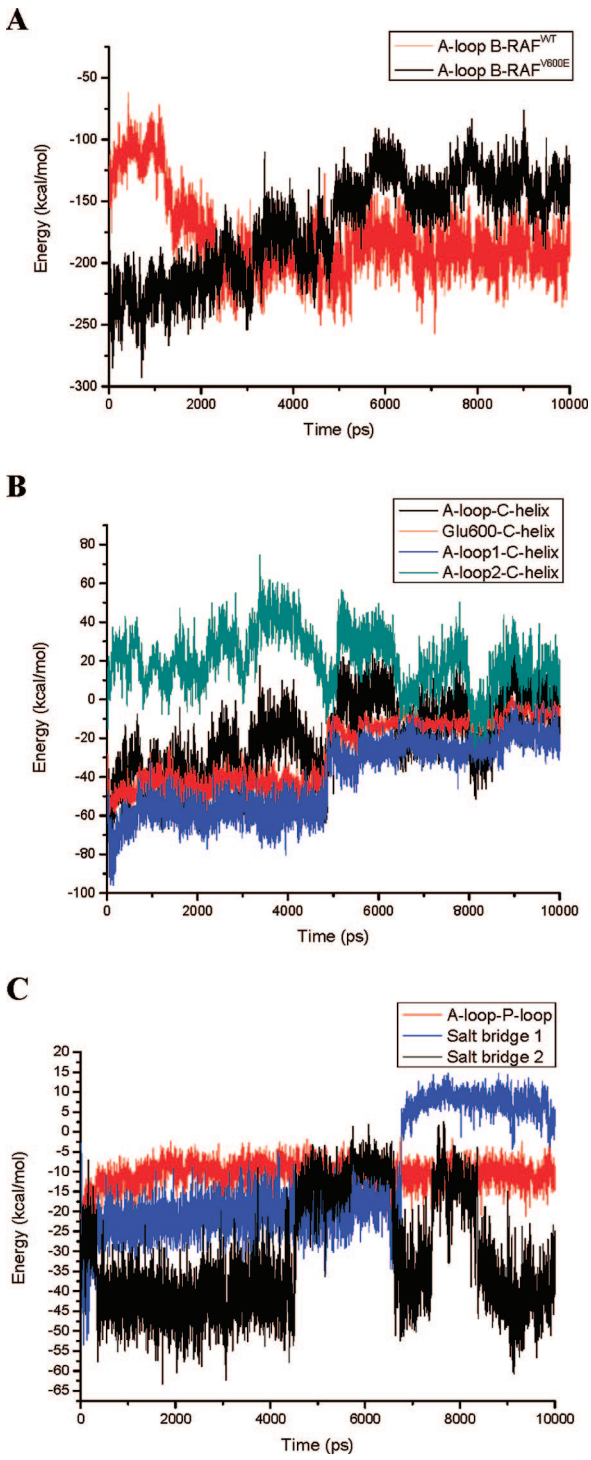


***Figure 8.*** (A) The electrostatic A-loop−protein interaction energies in B-RAF$^{WT}$ and B-RAF$^{V600E}$. (B) The electrostatic interaction energy between the A-loop and the C-helix, Glu600 and the C-helix, the A-loop-1 (residues 593−602, solved portion in the crystal structures) and the C-helix, the A-loop-2 (residues 603−611, not solved portion in the crystal structures) and the C-helix in B-RAF$^{V600E}$. (C) The Electrostatic interaction between the A and P-loops, the Asp594-Lys601 and Lys483-Glu501 ion pairs (salt bridge 1), and the Asp594-Lys601 and Asp576-Asn581 ion pairs (salt bridge 2).

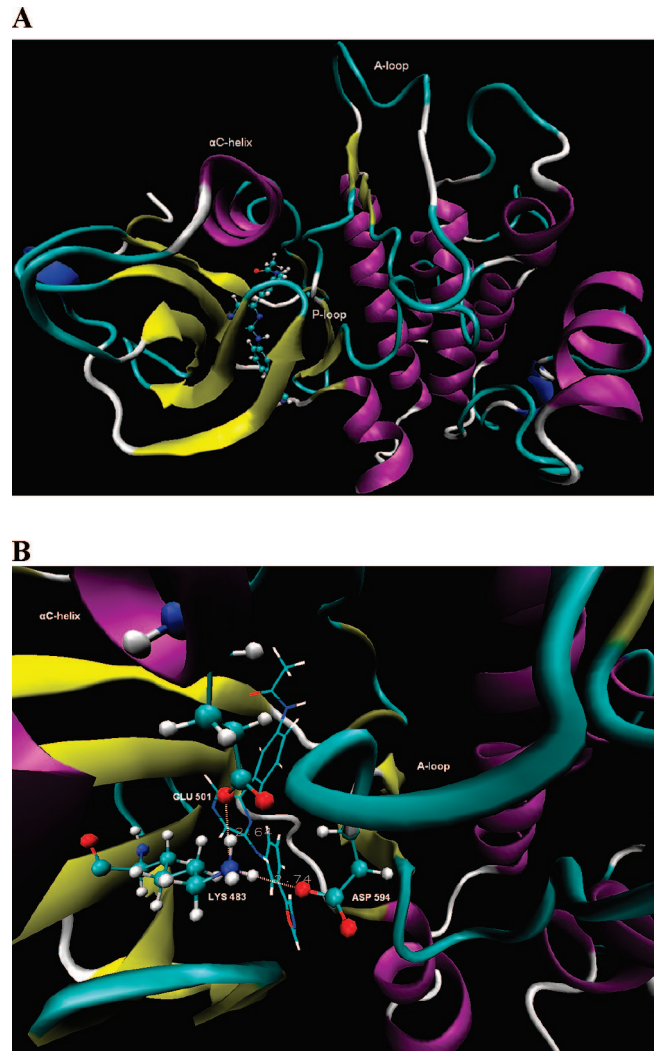


***Figure 9.*** (A) The conformation of B-RAF-A in a complex with ligand 1 after 10 ns of simulation. (B) A close look at the binding mode of ligand 1 in B-RAF-A.

the first 6 ns of the simulation time (see Figure 8A). Conversely, in the unbounded B-RAF$^{WT}$ the activation loop underwent stabilization and remained stable after 2 ns of the simulation (see Figure 8A). To obtain a detailed understanding of the destabilization of the activation segment in B-RAF$^{V600E}$ an analysis of the residues and their contribution to the A-loop interactions was performed.

Figure 8B shows the changes in the electrostatic interaction energies during the simulation time between the αC-helix, and the A-loop, Glu600, the A-loop-1 (residues 593−602, solved in the crystal structure) and the A-loop-2 (residues 603−611, not solved in the crystal structure), respectively. Figure 8C present the evolution of the electrostatic interaction energy between the A-loop and the P-loop, the Asp594-Lys601 and Lys483-Glu501 ion pairs (salt bridge 1) and the Asp594-Lys601 and Asn581-Asp576 ion pairs (salt bridge 2), respectively. Comparison of Figures 8B and 8C clearly indicates that the destabilization of the A-loop is mainly due to two factors, namely, the decrease of the electrostatic A-loop−αC-helix interactions and the interactions produced by the participants in the identified hydrogen bond network.

Presumably, these processes are linked because the strong decrease in the electrostatic interaction energy at 4.5−4.8 ns seen in Figure 8B occurred simultaneously with the decrease of the corresponding salt bridge 2 energy. During this time period, the Lys601 changed its conformation (4.5 ns) and the interaction energy between the Asp594-Lys601 and Asn581-Asp576 ion pairs decreased, most likely contributing to the Glu600 conformational change (4.8 ns) and the decrease in the Glu600−αC-helix interaction energy.

One can speculate that such energy evolution is due to the differences between the models obtained for the missing A-loop portion for B-RAF$^{WT}$ and B-RAF$^{V600E}$. However, the detailed interaction energy analysis showed that Glu600 and the Asp594-Lys601 ion pair gave the main contribution to the electrostatic changes in the A-loop−αC-helix interactions (see Figures 8B and 8C). These residues reside in the A-loop portion solved in the crystal structure (A-loop-1),[4] and thus the modeled A-loop portion should only play a minor role in these processes. The modeled portion of the A-loop had an average total energy of −3.0 kcal/mol for the first nanosecond, +7.8 kcal/mol for the period 0−5 ns and varied randomly during the simulation time (see Figure 8B). Conversely, during the first 5 ns, the A-loop-1 segment that was solved in the crystal structure had an average energy of −72.8 kcal/mol. Thus, the modeled A-loop portion contributed only to the fluctuations in the A-loop−αC-helix electrostatic energy, but gradually stabilized during the simulation, and does not qualitatively affect the conclusions above.

Our results showed that the A-loop−P-loop interactions were stable throughout the simulation in both B-RAF$^{WT}$ and B-RAF$^{V600E}$ (see Table 1 and Figure 8C), indicating that the P-loop is unlikely to have a contribution to the B-RAF$^{V600E}$ destabilization. These results demonstrate in a quantitative way that the A-loop−αC-helix interactions and the interactions between the participants in the network are presumably the major mechanism of the B-RAF$^{V600E}$ activation. The repulsive electrostatic forces between the A-loop, the αC-helix and the P-loop were identified as the main mechanism of B-RAF kinase activation in a previous MD study of the V600E and V599Ins mutants.[8] However, the relevant contributions of the αC-helix and the P-loop were not specified.

The data above indicate the important role of the electrostatic interactions between the participants in the hydrogen bond network provoking different conformation in the different kinase types. Thr599 and Asn581 were joined in this salt bridge network in both B-RAF$^{WT}$ and B-RAF$^{V600E}$. According to the results above it would be expected that the mutation of these residues will reorganize the interactions in the salt bridge network affect the catalytic residues and promote the kinase activation, explaining the experimentally observed increase in the activity. The phosphorylation of Thr599 will most likely dramatically change the conformation of the A-loop, which can explain why this process is needed for the wild type kinase activation.[54]

**3.2.6. Molecular Dynamics of B-RAF-A in Complex with Ligand 1.** Figures 9A and 9B show a possible binding mode for ligand 1 in B-RAF-A, which can explain the ligand selectivity to the inactive forms. A strong salt bridge between Lys483, Glu501 and Asp594 was identified and remained stable during the simulation. However, in contrast to the two inactive forms, the inhibitor does not form hydrogen bonds with the catalytic residues Lys483, Glu501, and Asp594 and thus it is not involved in strong hydrogen bond networks. Thus the conformation of the catalytic residues was not affected by the ligand binding. As shown in Table 2 the binding between ligand 1 and the active form of the kinase is not energetically favorable.

The crystal structures of the B-RAF-A showed that the main conformational differences in the binding site are present in the catalytic residues and the distances between the Lys483-Glu501 and Lys483-Asp594 ion pairs differ in the available crystal structures. The ligand 1 binding position in B-RAF-A was similar to that of the PLX4720 inhibitor in a recently obtained crystal structure,[6] but the compound was not involved in the electrostatic interactions with the salt bridge network which can explain the low selectivity to the active kinase form. PLX4720 binds to both inactive B-RAF$^{WT}$ and B-RAF-A, preferentially to the active form. The propyl group of this ligand was critical for the selective binding to the kinase active conformation.[6] According to the X-ray structure of PLX4720 in a complex with inactive B-RAF$^{WT}$ [6] and our MD model, the propyl group shifts the Glu501 conformation disrupting the interactions with Lys601. This most likely leads to unfavorable interactions with the other residues in the salt bridge network, contributing to the higher selectivity to B-RAF-A.

**3.3. LBE Analysis of the B-RAF$^{WT}$ Binding Site.** To obtain a quantitative and detailed understanding of the MD results, which indicated a similar ligand binding mode in the wild type and the mutant forms of the kinase, and more importantly to highlight the molecular basis of the ligand selectivity, the LBE approach was applied to search for potential correlations between the B-RAF$^{WT}$ ligand−protein interactions and the B-RAF$^{V600E}$ activity. First, one global energy parameter was calculated for each inhibitor in the B-RAF$^{WT}$ binding site, the ligand van der Waals binding energy. Second, the total (van der Waals plus electrostatic) LBEs of two molecular substructures were calculated for the same binding site. These are the C═O group within fragment 1 (see Figure 1) and the different R substituents plus the common N−H group (fragment 2 in Figure 1). Thus one of the selected substructures is common for all the inhibitors, whereas fragment 2 is different from one inhibitor to another. The LBE descriptors were selected based on the MD and MM-PBSA results, which indicated the significance of the

(54) Zhang, B. H.; Guan, K. L. Activation of B-Raf kinase requires phosphorylation of the conserved residues Thr598 and Ser601. *EMBO J.* **2000**, *19*, 5429–5439.

***Table 3.*** The Summarized LBE Results from Statistical Analysis Using MLR

| | MLR-1 | MLR-2 |
|---|---|---|
| | Training Set | |
| $r^2$ [a] | 0.83 | 0.83 |
| $q^2$ | 0.77 | 0.75 |
| RMSE | 0.24 | 0.25 |
| *N* | 26 | 18 |
| B-weight 1[b] | 0.61 | 0.60 |
| B-weight 2 | 0.46 | 0.48 |
| B-weight 3 | 0.39 | 0.40 |
| | Test Set | |
| $r^2_{pred}$ [c] | | 0.82 |
| $RMSE_{pred}$ | | 0.26 |
| *n* | | 8 |

[a] $r^2$, $q^2$, RMSE and *n* are the correlation coefficient, the cross-validated correlation coefficient using the leave-one-out method, the root-mean-square error, and the number of the ligands used (training and test set) in the models, respectively. [b] The standardized (B-weights) coefficients for the $LBE_{CO}$, $LBE_{fragment2}$ and $vdW_{Total}$ descriptors, respectively. [c] $r^2_{pred}$ is the correlation coefficient and $RMSE_{pred}$ is the root-mean-square error of the predictions for the test set compounds only.

ligand carbonyl group−Lys601 and the ligand amino group−Glu501 interactions in both B-RAF$^{WT}$ and B-RAF$^{V600}$, as well as the considerably higher contribution of the van der Waals binding energy. In this way, a simple but well-grounded set of 3 descriptors was built (see Table 2S in the Supporting Information).

The statistical analysis was carried out with the MLR techniques. For the first MLR model all ligands were included (MLR-1), whereas in the second MLR (MLR-2) analysis, the series was divided into training and test sets comprising 18 and 8 compounds, respectively. We selected the test set randomly. Figures 4S and 5S in the Supporting Information show the relationship between the ligand binding energies in B-RAF$^{WT}$ and B-RAF$^{V600E}$ activity for the training and test sets. Statistics of all the models are summarized in Table 3. The MLR-1 results showed that there is a strong relationship between the B-RAF$^{WT}$ ligand binding properties and the B-RAF$^{V600E}$ activity:

$$-\log IC_{50} = -7.438(0.651) - 0.618(0.088)LBE_{CO} - 0.044(0.009)LBE_{fragment2} - 0.042(0.01)vdW_{total} \quad (8)$$

where $LBE_{CO}$ and $LBE_{fragment2}$ are the LBEs of the carbonyl group and fragment 2 respectively, whereas $vdW_{total}$ is the total van der Waals binding energy of the compounds. In the parentheses the standard errors for each descriptor are shown. The statistical values for this correlation are comparable to those for the MLR-2 model (see Table 3). The Fisher's criterion for eq 8 is $F = 36.6$.

According to the above relationships the LBE of the carbonyl group is a major factor for the ligand activity and selectivity, which quantitatively describes its importance for all the compounds studied. Thus, these results confirm the significance of the interactions between the C═O group and Lys601 for inhibition of the inactive B-RAF, discussed in the previous paragraphs. The second significant descriptor is the LBE of fragment 2 which consists of the amino group that forms an hydrogen bond with Glu501 and the different substituents (R-groups) in the series, which were found to interact with the catalytic Lys483 and Asp594 residues (see Figures 3B, 5B and 1S and 2S in the Supporting Information). The LBE and the MD analyses demonstrate that the ligands participate in and disorder the identified salt bridge network while inhibiting both B-RAF$^{WT}$ and B-RAF$^{V600E}$. The $LBE_{CO}$ and $LBE_{fragment2}$ significance for the activity indicates that the reorganization of the Lys483-Glu501-Asp594-Lys601 interactions by the exclusion of the Asp594-Lys601 and the Lys483-Asp594 links produces changes in the ATP coordinating and catalytic residues that lead to inhibition (see also MD paragraphs). The importance of the van der Waals total energy demonstrates that the better occupation of this binding pocket and thus the restriction of the active segment flexibility is an important factor for the activity, as was proposed in the MD paragraph and supported by the MM-PBSA calculations.

## 4. Discussion

The LBE results support the data obtained by the MD and the MM-PBSA approaches and suggest that the selectivity of the ligands is related to the above-mentioned interactions, particularly those formed in the specific binding pocket where Lys601, Glu501, Asp594 and Lys483 play an important role. Ligand 1 forms stronger interactions with Lys601 and Glu501 in B-RAF$^{WT}$ than in B-RAF$^{V600E}$ (see Table 1) presumably provoking the destabilization of the catalytic residues, which leads to the stronger inhibition and better selectivity to the wild type kinase in accordance with the MM-PBSA results. However, these interactions despite their difference in magnitude were present in both B-RAF$^{WT}$ and B-RAF$^{V600E}$ providing an explanation of the strong correlation found by the LBE method. Presumably, this mechanism of the inactive B-RAF selectivity is neither unique for the compounds studied nor unique for the kinase. The urea group of sorafenib forms two hydrogen bonds with the protein, one via its amide nitrogen atom to the carboxylate side chain of the Glu501 residue and the second via the carbonyl moiety to the main chain nitrogen of Asp594.[4] A hydrogen bond between Glu501 and the amide group in a series of recently developed inhibitors was also identified.[6] The propyl group of the recently discovered inhibitor PLX4720 produces a large shift in the Glu501 conformation, indicating the significance of this interaction in the inactive B-RAF binding pocket, and was defined as critical for the selectivity of the ligand toward B-RAF-A.[6] The equivalent constellation of hydrogen bonds contributes to the interactions between the c-Abl and p38 MAP kinases and their respective inhibitors STI-571 and BIRB-796.[55−57]

During the preparation of our manuscript, experimental data for the activity of a new series diarylimidazole inhibitors to both inactive B-RAF$^{WT}$ and B-RAF$^{V600E}$ kinase forms was published.[51] To our knowledge this was the first study

of a series of inhibitors that provides information for the selectivity to these kinases. The observed $IC_{50}$ values of the 13 compounds were in the range of 0.007−0.887 $\mu$M for B-RAF$^{WT}$ and 0.002−0.274 $\mu$M for B-RAF$^{V600E}$. We found that there was a strong correlation between the measured activities of the wild type and mutant kinase ($r^2 = 0.94$, SE $= 0.07$, $F = 176$ and $n = 13$), which strongly supports the results presented here. Moreover, the molecular modeling results identified a hydrogen bond with Glu501 as an important factor for ligand binding,[51] suggesting that the proposed mechanism of the compounds selectivity presented here is not unique for the studied series of inhibitors based on a disubstituted pyrazine scaffold.

According to our results, Lys601 and Glu501 are seen to have a significant role for the activity and selectivity of the ligands. Also, these residues contribute to the B-RAF$^{WT}$ stabilization through the interactions between the αC-helix and the A-loop as well as between the residues in the identified unique salt bridge network. Conversely, in B-RAF$^{V600E}$ the electrostatic interactions between the αC-helix and the A-loop and in particular interactions involving the Glu600 and Lys601 residues were the identified as major factors for the mutant destabilization. The important role of Lys601 in B-RAF$^{WT}$ was highlighted in both the protein in a complex and in its unbounded state, suggesting a molecular basis of experimentally observed high increase of the kinase activity by the K601E mutation.

It should be mentioned that available literature data on the inhibition of these kinases is still rather limited. However, strong similarities were observed between the binding mode of the set of inhibitors studied in this paper and several other ligands reported to inhibit the studied B-RAF forms up to now.

The results from LBE analyses demonstrate also some of the advantages of this approach in conjunction with MD analysis. First, it can be used to estimate the significance of individual substituents and their contribution to the observed activities. Second, a more clear biochemical interpretation of the ligand binding mode can be obtained compared with studies that only use the total binding energy parameters as descriptors.

The results from the present paper can be helpful in the design of new inhibitors with higher V600E selectivity, as well for the better understanding of the molecular processes of the B-RAF stabilization and destabilization.

**Acknowledgment.** F.F. and S.Ó.J. acknowledge financial support from Research Council for Technology and Production Sciences and the Program Commission on Nanoscience, Biotechnology and IT (NABIIT). F.F. and I.P. acknowledge the partial support of the Bulgarian National Council for Scientific Research. Thanks are due to R. Rusev, J. Adlangijski and O. Taboureau for the helpful discussion.

**Supporting Information Available:** Supplementary Figures 1S−5S and Tables 1S and 2S as described in the text. This material is available free of charge via the Internet at http://pubs.acs.org.

MP8001107

(55) Nagar, B.; Bornmann, W. G.; Pellicena, P.; Schindler, T.; Veach, D. R.; Miller, W. T.; Clarkson, B.; Kuriyan, J. Crystal structures of the kinase domain of c-Abl in complex with the small molecule inhibitors PD173955 and imatinib (STI-571). *Cancer Res.* **2002**, *62*, 4236–4243.

(56) Pargellis, C.; Tong, L.; Churchill, L.; Cirillo, P. F.; Gilmore, T.; Graham, A. G.; Grob, P. M.; Hickey, E. R.; Moss, N.; Pav, S.; Regan, J. Inhibition of p38 MAP kinase by utilizing a novel allosteric binding site. *Nat. Struct. Biol.* **2002**, *9*, 268–272.

(57) Schindler, T.; Bornmann, W.; Pellicena, P.; Miller, W. T.; Clarkson, B.; Kuriyan, J. Structural mechanism for STI-571 inhibition of abelson tyrosine kinase. *Science* **2000**, *289*, 1938–1942.